Charge asymmetric dissociation of a CO^+ molecular-ion beam induced by strong laser fields

Nora G. Kling, J. McKenna, A. M. Sayler, B. Gaire, M. Zohrabi, U. Ablikim, K. D. Carnes, and I. Ben-Itzhak
J. R. Macdonald Laboratory, Physics Department, Kansas State University, Manhattan, Kansas 66506, USA
(Received 12 November 2012; published 22 January 2013)

Charge asymmetric dissociation into $C^{2+} + O$ following ionization of a CO^+ molecular-ion beam with intense ultrashort (7–40-fs) laser pulses is studied using a coincidence three-dimensional momentum imaging method. The data suggest that allowing the molecule enough time to stretch within a laser pulse such that it ionizes beyond the curve crossings of the $C^{2+} + O$ and $C^+ + O^+$ potentials enhances the otherwise hard-to-reach charge asymmetric dissociation channel.

DOI: 10.1103/PhysRevA.87.013418 PACS number(s): 32.80.Wr, 34.80.Gs

I. INTRODUCTION

The advent of ultrashort laser-pulse generation has allowed the examination of the dynamics of processes, such as ionization and dissociation of molecules. This has led to breakthroughs in our understanding of light-dressed potentials, bond softening, and multielectron dissociative ionization, to name only a few [1–4]. Detection and imaging technologies have also been advancing, permitting a more detailed look into the kinematics of fragmentation processes. For example, relevant to this paper, we investigate molecular-ion beams and can, therefore, detect neutral fragments [5]. This provides kinematically complete information for dissociation, whereas, for dissociative ionization, the electron's momentum is not determined, limiting the kinematic information to the "atomic fragments." Here, we investigate the pulse duration and intensity dependence of laser-induced charge asymmetric dissociation (CAD) of CO^+.

Charge asymmetric dissociation refers to the uneven charge sharing between dissociating fragments of a molecular ion. For example, the possible dissociation channels of an AB^{2+} molecular ion are charge symmetric dissociation (CSD), i.e., $A^+ + B^+$or CAD, i.e., $A^{2+} + B$ or $A + B^{2+}$, where A^{i+} and B^{j+} represent the two-body fragments of any diatomic or polyatomic molecule. Throughout this paper, we refer to the channels by the final charge states of the fragments (i, j) where the less massive fragment is listed first.

It is well established that the fragments of rapidly formed transient highly charged molecular ions tend to have a symmetric charge distribution [6,7]. For example, collisions of fast F^{4+} (at 1 MeV/amu, i.e., tens of attoseconds collision times) with CO produce multiple charge states CO^{q+} by sudden ionization (also referred to as "vertical transitions") that preferentially break into equally charged carbon and oxygen fragments in the ensuing unimolecular dissociation. This is demonstrated by Ben-Itzhak *et al.* [6] by the measured distribution of the charge carried by the oxygen fragment shown in Fig. 1. For both CO^{2+} and CO^{4+}, the peak occurs when the charge is shared evenly between the carbon and the oxygen fragments. More importantly, for this paper, the branching ratio falls off rapidly as the charge sharing becomes more asymmetric, meaning that the more asymmetric the charge sharing, the less likely the channel is to occur [6,8].

Heuristically, CSD ought to be the favorable channel as electron motion is much faster than the time scale for dissociation, and therefore, the charge can rearrange faster than the two nuclei move apart. Furthermore, states crossing the CAD states and leading to CSD (such as the $^1\Pi$ state shown in Fig. 2) typically lie lower in energy than CAD states at larger R. Thus, molecules are more likely to transition from CAD to CSD channels as the molecule stretches leading to a predominance of CSD as depicted by the arrows in Fig. 2. Moreover, molecules ionized at larger R will favor the lower-lying CSD state. These reasons, combined, contribute to the observed propensity for CSD over CAD.

Although the conditions for producing CAD seem unfavorable, it has been observed as weak dissociation channels for many molecules ionized by weak and strong fields [9–20]. Mulliken [21] proposed that CAD states can be reached from CSD states by means of a charge transfer transition, i.e., $A^+ + B^+ \rightarrow A^{2+} + B$ [22,23]. In one case, Gibson *et al.* experimentally studied both charge symmetric and asymmetric breakup channels of I_2 and found that CAD of multiply charged states of I_2^{q+}, up to I_2^{10+}, are most likely due to populating the charge transfer states [15], e.g., populating the $I^+ + I^+$ states that later undergo charge exchange to form the asymmetric $I^{2+} + I$ final products. A later report by Guo *et al.* stresses that charge transfer is not the cause for CAD states to be populated in smaller molecules, such as N_2 and O_2 as the charge asymmetric dipole coupling cannot provide sufficient energy to populate the CAD states from the CSD states [13].

CAD has been observed in the strong-field regime for a large range of pulse durations (6 fs – 10 ps) [13–20]. The CSD channel is always dominant, especially with longer laser pulses at ∼800-nm wavelengths, i.e., pulses long enough to reach the critical internuclear distance where enhanced ionization occurs. CAD channels, such as the (2,0) channels for O_2 and N_2 [13] and for CO [14], are more visible at shorter pulse widths (30 and 6 fs, respectively), but a systematic study has yet to be performed. That leaves the question: What happens to the likelihood of the CAD channel with decreasing pulse duration, exactly the question we are addressing in this paper.

All previous laser studies of CAD start from a neutral molecular target. Therefore, neutral fragments have not been measured, and CAD of dications, i.e., the (2,0) channel, is inferred from the data either by a process of elimination to identify which ions go with the undetectable neutral fragment or by taking advantage of the different kinetic-energy release (KER) range expected for the CAD channel (typically, one assumes that the doubly charged ion from a (2,0) channel is much less energetic than the one from the (2,1) channel). This

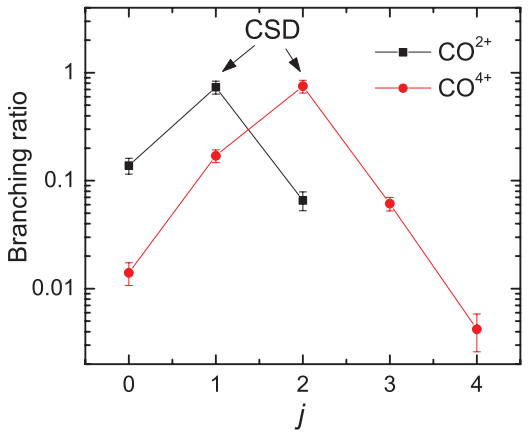

FIG. 1. (Color online) Branching ratio of the dissociation channels of transient CO^{q+} produced by 1-MeV/amu F^{4+} ion impact on CO, specifically for $CO^{q+} \rightarrow C^{i+} + O^{j+}$ for $q = 2$ and 4 and $i = q - j$, adapted from Ref. [6] with lines added for visualization. The branching ratio is defined as the fraction of a specific breakup channel $C^{i+} + O^{j+}$ from the total of all channels associated with the same transient ion CO^{q+}. Both charge distributions indicate that symmetric charge breakup is preferential and that CAD is significantly smaller. Note that the contribution shown for $q = 2$ does not add up to 1 as there is also a fraction in the long-lived CO^{2+} ion, which is unaccounted for here.

may leave some doubts about the validity of the assignment of the CAD channel. The unambiguous measurement of the (2,0) channel requires measuring a charged fragment in coincidence with a neutral fragment.

Using an ion beam as the target, we overcome this experimental challenge, as the neutral fragment carries a fraction of the beam energy, typically a few keV and, therefore, can be efficiently detected. Having the capability to measure the neutral fragment gives us the advantage of performing a near-kinematically complete measurement (we do not detect the ionized electron, which takes away very little momentum), leaving no doubt about the identity of the observed CAD and CSD channels and avoiding any *a priori* assumptions about the expected KER.

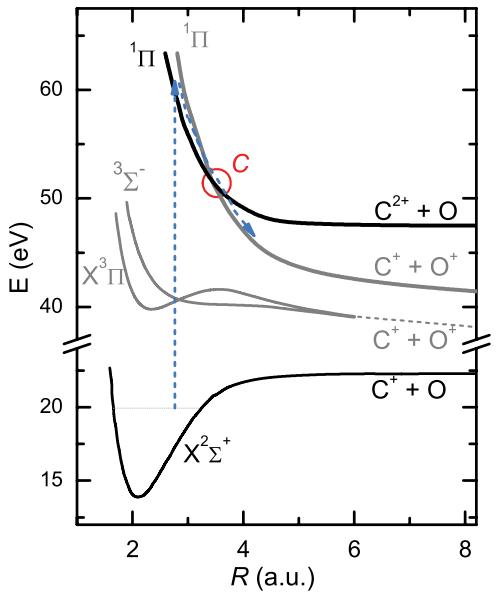

FIG. 2. (Color online) Potential-energy curves for selected states of CO^+ and CO^{2+} from Refs. [24,41,42]. The pathway depicted by the arrows shows that, although the (2,0) channel can initially be populated, there is a propensity to dissociate onto the (1,1) channel, facilitated by charge transfer at the curve crossing (circle marked *C*) between the (2,0) and the (1,1) states (see text).

In this paper, we chose to study CAD of CO^{2+} formed by strong-field ionization of a CO^+ parent molecular-ion beam for the convenient fact that potential-energy curves (PECs) dissociating into $C^{2+} + O$ have already been calculated [24,25]. It is important to note that calculations of such highly excited states of molecular ions are extremely demanding, and therefore, they are rather scarce. Specifically, we investigated the probability of dissociation via the (2,0) and (1,1) channels as a function of pulse duration 7–40 fs and intensity $\sim(1 - 6) \times 10^{15}$ W/cm^2. We find no measurable signal for the (0,2) CAD channel (see later discussion). Interestingly, we find that the (2,0) channel is more likely for the longer pulses considered. We suggest that, with longer pulse durations, the molecule has more time to stretch beyond the curve crossings with the CSD states before ionizing to the CAD states.

II. EXPERIMENT

We create a CO^+ ion beam in an electron cyclotron resonance (ECR) ion source and direct it through a longitudinal spectrometer where it crosses a laser beam as shown schematically in Fig. 3(a). The spectrometer provides a static field in the interaction region, which accelerates charged fragments and, therefore, assists in separating species with different charge-to-energy ratios, allowing for their identification via their coincidence time of flight (TOF), see Fig. 3(b). Beam fragments are detected by a microchannel plate detector with a delay line anode from which both timing and position information are recorded on a single shot basis. A small Faraday cup is placed in front of the detector to collect the ion beam, and the current is recorded such that spectra from different runs can be normalized to each other for comparison. This method is known as coincidence three-dimensional (3D) momentum imaging (for a more detailed description see Refs. [5,26]).

For the data acquired with 30-fs pulse duration, an additional transverse electrostatic field was applied after the spectrometer and before the detector to measure molecular ions with higher charge states than the parent ion beam [27,28]. Otherwise, the setup was similar for all of the collected data.

Our laser pulses were provided by the Kansas Light Source, which outputs 2-mJ 40-fs (full width at half maximum) pulses at a 1-kHz repetition rate centered about 790 nm [29]. By sending the pulses through a neon-filled hollow-core fiber and a chirped-mirror compressor, we generate 7-fs pulses. Reducing the amount of neon in the hollow-core fiber and adjusting the corresponding amount of fused silica chirp compensation, 15-fs pulses are achieved. All pulse durations are measured by frequency-resolved optical gating (FROG). The linearly polarized pulses with the desired pulse duration are then focused onto the ion beam in the interaction region within the spectrometer by an off axis $f = 203$-mm parabolic

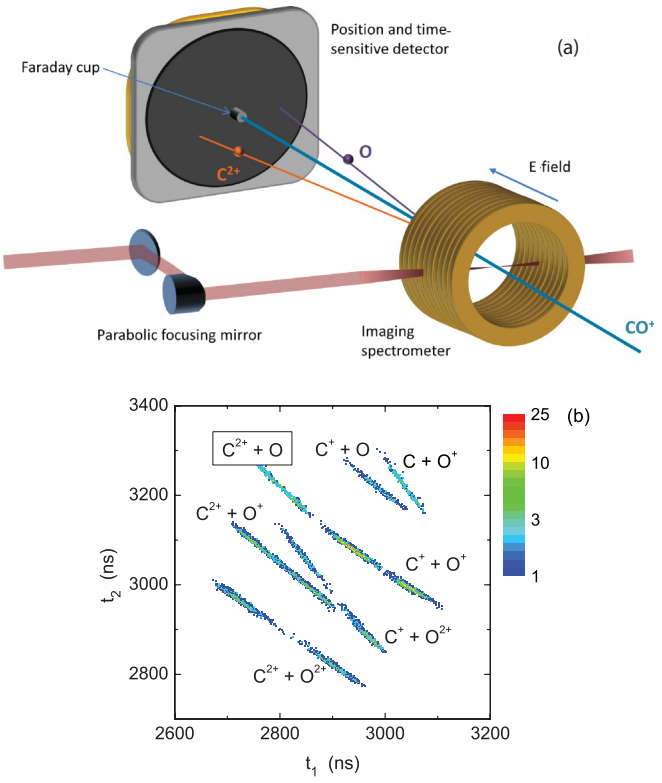

FIG. 3. (Color online) (a) Schematic of the experimental setup and (b) coincidence time-of-flight map of the various channels of CO^+ fragmentation from interaction with 40-fs 7×10^{15}-W/cm^2 pulses with the CAD channel highlighted.

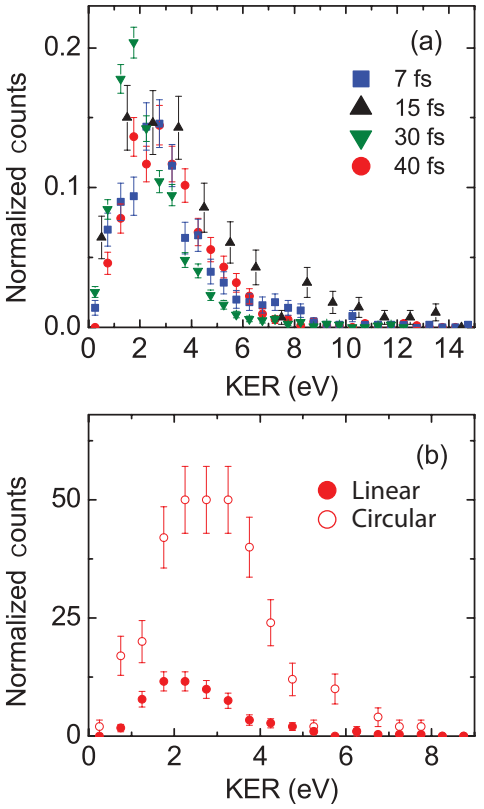

FIG. 4. (Color online) KER distributions for $CO^+ \rightarrow C^{2+} + O$ fragmentation in (a) 7-, 15-, 30-, and 40-fs laser pulses with intensities of 7.0, 5.0, 6.0, and 7.2×10^{15} W/cm^2, respectively, and in (b) 40-fs pulses with 3.6×10^{15} W/cm^2 for linear polarization and 7.2×10^{15} W/cm^2 for circular polarization. The linear and circular polarization pulses are normalized to each other as outlined in the main text. The higher rate of $C^{2+} + O$ events for circular polarization suggests that electron recollision does not play an important role in this CAD process.

mirror. Adjusting the position of the focusing mirror allows us to select which peak intensity overlaps the thin ion beam ($\sim 0.8 \times 0.8\,\text{mm}^2$). By imaging the laser beam profile on a charge-coupled device (CCD) camera, we also determine the laser spot size and can account for it in the normalization procedure such that different measurements can be quantitatively compared to each other.

To generate circular polarization, when relevant, we use a broadband quarter-wave plate, carefully adjusting the beam path by removing glass to ensure no chirp is added to the otherwise transform-limited pulses. The circularly polarized pulses are characterized by matching the power of the *p* and *s* components of the laser beam when sent through a polarizing cube beam splitter. To match the maximum electric-field strength for circular and linear polarizations, we adjusted the position of the focusing mirror such that the intensity for the circular polarization was twice the value for the linear polarization.

In this paper, we focus on the dissociation channels of the transient CO^{2+} produced by ionizing the primary CO^+ beam. Specifically, we compare the charge symmetric dissociative ionization into $C^+ + O^+$ to the charge asymmetric fragmentation into $C^{2+} + O$. Figure 3(b) shows the coincidence TOF map for all fragmentation channels of CO^+ resulting from the interaction with the laser. Each channel is cleanly separated from the others, forming a straight line due to momentum conservation. The channels of interest, (1,1) and (2,0), measured simultaneously, are then separated using this coincidence map and are analyzed individually.

III. RESULTS AND DISCUSSION

The measured KER distributions of $C^{2+} + O$ breakup for 7-, 15-, 30-, and 40-fs pulses are shown in Fig. 4(a). For all pulse durations, the KER distributions peak at about 2.5 eV and have similar shapes. The KER distributions for linear- and circular-polarized 40-fs pulses are compared in Fig. 4(b). These spectra are normalized to each other by accounting for the differences in the ion-beam current and the laser spot size for each data set. The yield is not suppressed with circular polarization suggesting that the driving mechanism, for this set of laser parameters, does not involve an electron recollision process. One would expect the signal strength to decrease significantly for circular polarization if a recollision step plays an important role [30].

In order to explain the observed KER, we consider the PECs of CO^{2+} leading to CAD and CSD states. Although it is a great challenge to calculate potential-energy curves for CAD states as they are highly excited states of a molecular dication, Polák and Čížek [24] and Levasseur *et al.* [25] have

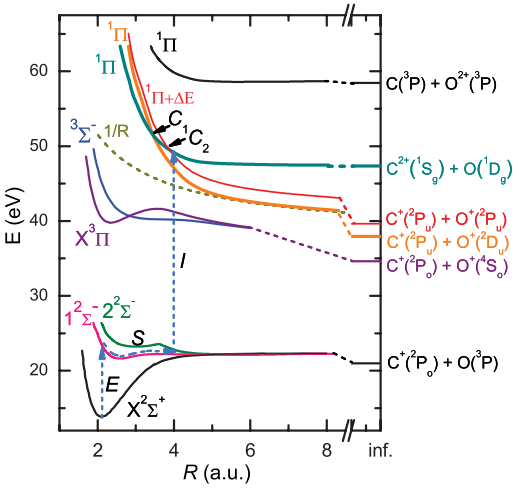

FIG. 5. (Color online) Potential-energy curves of select states of CO^+ and CO^{2+} from Refs. [24,41,42]. The dashed arrow sequence [excite (E), stretch (S), and ionize (I)] indicates a proposed pathway for reaching the (2,0) CAD channel (see text). We also show schematically the $^1\Pi$ CO^{2+} curve linked to the $C^+(^2P_u) + O^+(^2P_u)$ dissociation limit to indicate the sequence of crossings. This curve is constructed by adding the energy difference, $\Delta E = O^+(^2P_u) - O^+(^2D_u)$, to the $^1\Pi$ CO^{2+} curve shown with the limit $C^+(^2P_u) + O^+(^2D_u)$.

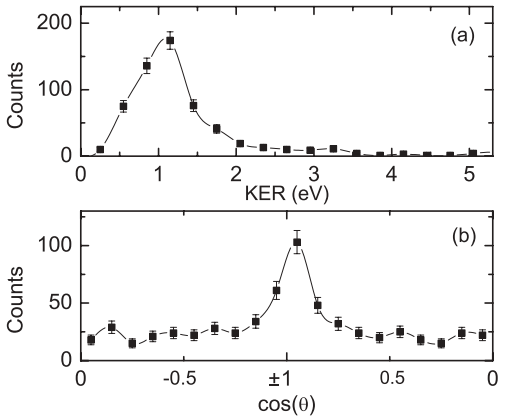

FIG. 6. The (a) KER and (b) angular distributions for the $C^+ + O$ dissociation channel with linearly polarized 40-fs 3.6×10^{15}-W/cm^2 pulses.

evaluated the PECs leading to CAD for CO^{2+}. Intuitively, the (2,0) curves are expected to be strongly repulsive (i.e., steep) at small internuclear distance R and become weakly bound at large R due to the attraction between the doubly charged fragment and the polarized neutral fragment. On the other hand, the PECs associated with the (1,1) channel are highly repulsive at large R due to the Coulomb repulsion between the C^+ and the O^+ fragments. This, combined with the fact that the dissociation limit of the (1,1) channel is lower than the (2,0) channel, leads to curve crossings between the states leading to the (2,0) and (1,1) channels for all state symmetries considered by Polák and Čížek [24] and Levasseur *et al.* [25] as depicted for one case in Fig. 2.

These PECs are coupled at the crossings (marked "C_n" in Fig. 5) where population can be transferred from the (2,0) channel to the (1,1) channel. It is important to note that there are a multitude of similar crossings between the lowest (2,0) state and the manifold of (1,1) states dissociating into excited C^+ or O^+ fragments (only the first couple of crossings are shown in Fig. 5 for clarity). The transition rates at these crossings can be evaluated, for example, by using the Landau-Zener theory [31,32]. It is expected that the coupling between these states leading to CAD and CSD becomes weaker with increasing R [25]. Therefore, we hypothesize that efficient population of the (2,0) channel proceeds via a two-step process. First, the CO^+ ion is excited to a dissociating state of CO^+, thus, initiating a stretch of the internuclear distance. Then, ionization occurs, and the fraction ending on the (2,0) state has a higher chance of avoiding transitions to CSD states if R has already stretched beyond the critical crossings depleting the CAD state. This scenario, depicted schematically in Fig. 5, is discussed in further detail before we test it with our experimental data.

Inspection of the $C^+ + O$, i.e., (1,0), dissociation channel's KER and angular distribution gives insight into the first step, that is, how the stretching might occur. Assuming that not all of the population of the excited CO^+ state ionizes, some of the population dissociates on that state. The angular distribution of the (1,0) channel for linearly polarized 40-fs 3.6×10^{15}-W/cm^2 pulses, shown in Fig. 6(b), peaks around $\cos\theta = \pm 1$, where θ describes the angle between the polarization of the laser and the dissociation direction. This dissociation along the laser polarization suggests no angular momentum change during the excitation, i.e., $\Delta\Lambda = 0$ [33,34]. Hence, for the (1,0) channel, dissociation must be along a curve with Σ symmetry in order to match the symmetry of the ground CO^+ $X\ ^2\sum^+$ state: The most likely candidates are the $1\ ^2\sum^-$ and $2\ ^2\sum^-$ states of CO^+, also shown in Fig. 5.

Taking advantage of the KER information for the (1,0) channel, shown in Fig. 6(a), we can select the $1\ ^2\sum^-$ state as the best match to the data because the measured KER distribution is centered around 1 eV as expected for the $1\ ^2\sum^-$ state dissociating from about R_0 of CO^+. In contrast, dissociation along the $2\ ^2\sum^-$ state would yield a KER of about 4 eV, which is clearly inconsistent with the dissociation data.

Once the PEC for the dissociation step has been determined, we evaluate, using classical propagation, the time needed to reach a given R when starting from the equilibrium distance, R_0, of the parent molecule CO^+. The results, shown in the inset of Fig. 7, indicate that R can double from its initial value R_0 within about 20 fs, which is on a time scale less than our longer pulses and more than the shorter ones used here.

One may question why we use R_0 of the CO^+ as the initial point since that point could be affected by vibrational excitation. This assumption is justified by the fact that the bond length of CO and CO^+ are similar to each other (see Fig. 7) at 2.132 and 2.107 a.u., respectively [35]. As a result, the Franck-Condon distribution of CO^+ vibrational states, produced in the ion source by fast electron impact ionization, peaks near the bottom (around $v = 1$) of the CO^+ potential well. Further multiphoton excitations to the $1\ ^2\sum^-$ or $2\ ^2\sum^-$ state are not expected to change the initial R significantly.

Next, we estimate the location in R where the ionization step occurs from the observed KER of the (2,0) channel and the

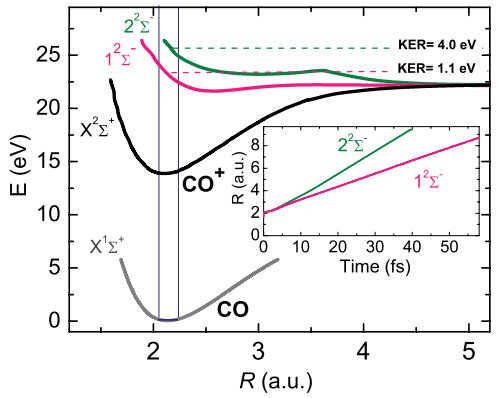

FIG. 7. (Color online) Potential-energy curves for CO ($X\ ^1\Sigma^+$, gray line, from Ref. [43]) and CO^+ ($X\ ^2\Sigma^+$, black line, from Ref. [42]) ground states and two excited-state curves ($1\ ^2\Sigma^-$, pink and $2\ ^2\Sigma^-$, green, from Ref. [42]). The inset shows the classical calculation for propagation times along the $2\ ^2\Sigma^-$ and $1\ ^2\Sigma^-$ curves starting from R_0 of CO^+.

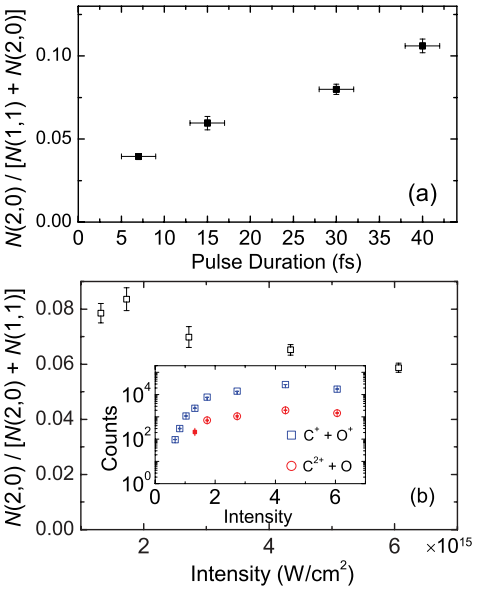

FIG. 8. (Color online) The CAD branching ratio $N(2,0)/[N(2,0)+N(1,1)]$ versus (a) pulse duration for an approximately constant intensity of $(5.0-7.2)\times10^{15}$ W/cm^2 and (b) intensity with constant pulse duration of 30 fs. The inset in panel (b) shows the number of counts versus intensity for the individual channels as indicated. Error bars denote statistical error. Note that the pulse duration measurement resolution is ± 2 fs.

PECs leading to CAD from Ref. [24] (we choose these PECs because they extend to larger R and include the dissociation limit, thus, facilitating KER calculations). We select the $^1\Pi$ (2,0) state of CO^{2+} for illustration purposes (see Fig. 5). For this final state of CO^{2+}, ionization at $R = 4$ a.u. leads to the observed KER of 2.5 eV. Specifically, about 1 eV is gained by the dissociating CO^+ on its $1\ ^1\Sigma^-$ PEC, whereas, the rest is gained on the $^1\Pi$ state of CO^{2+} (both excitation and ionization steps are marked by vertical arrows in Fig. 5). According to the classical propagation calculation, it takes approximately 17 fs to stretch to an R of 4 a.u. on the $1\ ^2\Sigma^-$ state of CO^+. If the laser pulse is still intense enough to ionize this excited state of CO^+ to CO^{2+} once $R \sim 4$ a.u. is reached, there is some probability of getting onto the $^1\Pi$ state of CO^{2+} that leads to the (2,0) channel (see Fig. 5). The chances of this state reaching the $C^{2+} + O$ dissociation limit are higher because the main crossings leading to charge transfer transitions $C^{2+} + O \rightarrow C^+ + O^+$ are at smaller R of about 3.5 a.u.

Therefore, according to our proposed model, depicted by the sequence of arrows in Fig. 5, the pulse duration needs to be longer than 17 fs to maximize the abundance of the CAD channel. However, if the pulse duration is too long, enhanced ionization can take over, which again prefers the CSD products—indicating there is a window of pulse durations where CAD can occur with higher probability. Note that, in this context, it does not matter what the mechanism responsible for enhanced ionization is. A couple of possibilities are charge resonance enhanced ionization [36] and resonance enhanced multiphoton ionization [37,38].

Experimentally, to test our proposed mechanism, we evaluate the CAD branching ratio, $N(2,0)/[N(2,0)+N(1,1)]$, where $N(i,j)$ is the number of observed counts for channel (i,j). This branching ratio, as a function of pulse duration and peak intensity, is shown in Fig. 8. For the branching ratio versus pulse duration dependence in panel (a), the intensity is approximately constant at $(5.0-7.2)\times10^{15}$ W/cm^2, and for the plot depicting the branching ratio as a function of intensity, shown in panel (b), the pulse duration is fixed at 30 fs. Although detection efficiencies are not included in the CAD branching ratio evaluation, we expect them to approximately cancel each other as the (2,0) channel suffers from the lower efficiency of the neutral oxygen but benefits from the higher efficiency of the doubly charged carbon. Meanwhile, the C^+ and O^+ fragments will have similar efficiencies in between the efficiencies of the C^{2+} and O fragments [28].

As expected from our suggested mechanism, the measured CAD branching ratio defined above increases with increasing pulse duration over the range of our measurements because the CO^+ has more time to stretch and to ionize to the CAD state beyond the critical curve crossing(s) with the CSD state (labeled C_n in Fig. 5). This increases the survival rate of the CAD channel by reducing the charge transfer that depletes the CAD population. We expect the CAD branching ratio to start decreasing once the enhanced ionization kicks in because of a higher ionization rate to $C^+ + O^+$ by this mechanism, but this is expected beyond 65 fs according to Ref. [39]—which is beyond the extent of our data. This time scale is verified by our classical calculation of the time evolution of CO^+ dissociation shown in the inset of Fig. 7.

In contrast to the pulse duration dependence above, the CAD branching ratio tends to decrease slowly with increasing intensity as shown in Fig. 8(b). This trend is also consistent with the proposed mechanism and for similar reasons. For a fixed pulse shape (duration), the time difference between the CO^+ excitation step, which requires six photons (at 790 nm) and, therefore, a high laser intensity, and the ionization step becomes shorter with increasing intensity. This is due to the typical shift in ionization to smaller R with increasing laser intensity as the stronger field can bridge the increasing energy gap at smaller R [40].

Before closing, one may wonder why the other CAD channel, namely, dissociative ionization into $C + O^{2+}$, is not observed in our data and how this is consistent with our interpretation of the CAD mechanism. The main reason for the lower (0,2) rate is the fact that the PEC, leading to this CAD channel, is much higher in energy due to the higher IP of oxygen relative to carbon (by more than 11 eV). Therefore, a larger number of photons is needed to ionize to this CAD state, making it much less likely (see Fig. 5). However, that cannot be the whole story as we observe even higher ionization levels in our data, see the (2,1), (1,2), and (2,2) channels in Fig. 3(b), and further work is needed to explain the dominance of multiple ionization over this charge asymmetric dissociative ionization.

IV. SUMMARY AND OUTLOOK

Using a coincidence 3D momentum-imaging technique, we unambiguously studied the (2,0) CAD channel of CO^{2+} using a CO^+ ion-beam target. Contrary to earlier findings that CAD is easier to produce (from CO) with decreasing pulse duration, we find the CAD branching ratio, namely, $N(2,0)/[N(2,0) + N(1,1)]$ decreases with decreasing pulse duration below 40 fs. Furthermore, this CAD branching ratio decreases slightly with increasing intensity. The present measurements suggest that the CO^+ stretches on an excited state before ionizing onto the $^1\Pi$ state (or other CAD states) of CO^{2+}, which leads to the (2,0) channel. Most important is the fact that, in this mechanism, ionization to the CAD state happens at a larger internuclear distance than the charge-transfer crossing with the CSD state, therefore, suppressing the depletion of the CAD population by $C^{2+} + O \rightarrow C^+ + O^+$ charge-transfer transitions.

A rigorous way to test the proposed CAD mechanism would be to perform a pump-probe measurement. One could use a CO^+ or CO^{2+} beam as the target molecular ion. The latter likely will give a cleaner signal, whereas, the former will be less technically challenging. A short ($\leqslant$5-fs) pump pulse would need to initiate the stretching, whereas, a delayed short probe pulse would be utilized to populate the CAD channel. By varying the delay between the two pulses, the time evolution could be studied in detail giving insight into the dynamics of the curve crossings between states leading to CSD and CAD where charge transfer is predicted to occur.

ACKNOWLEDGMENTS

We are indebted to Z. Chang's group for providing expertise with the laser beams and to C. W. Fehrenbach for his help with the ion beams. We also are grateful to B. D. Esry for insightful discussions on this paper. This work was supported by the Chemical Sciences, Geosciences, and Biosciences Division, Office of Basic Energy Sciences, Office of Science, US Department of Energy.

[1] P. H. Bucksbaum, A. Zavriyev, H. G. Muller, and D. W. Schumacher, Phys. Rev. Lett. **64**, 1883 (1990).
[2] C. Cornaggia, J. Lavancier, D. Normand, J. Morellec, and P. Agostini, Phys. Rev. A **44**, 4499 (1991).
[3] C. Wunderlich, E. Kobler, H. Figger, and T. W. Hänsch, Phys. Rev. Lett. **78**, 2333 (1997).
[4] J. H. Posthumus, Rep. Prog. Phys. **67**, 623 (2004).
[5] I. Ben-Itzhak, P. Q. Wang, J. F. Xia, A. M. Sayler, M. A. Smith, K. D. Carnes, and B. D. Esry, Phys. Rev. Lett. **95**, 073002 (2005).
[6] I. Ben-Itzhak, S. G. Ginther, and K. D. Carnes, Phys. Rev. A **47**, 2827 (1993).
[7] K. Wohrer, G. Sampoll, R. L. Watson, M. Chabot, O. Herber, and V. Horvat, Phys. Rev. A **46**, 3929 (1992).
[8] K. Codling, L. J. Frasinski, and P. A. Hatherly, J. Phys. B: At. Mol. Opt. Phys. **22**, L321 (1989).
[9] P. Franceschi, D. Ascenzi, P. Tosi, R. Thissen, and J. Žabka, J. Chem. Phys. **126**, 134310 (2007).
[10] W. Eberhardt, E. W. Plummer, I. W. Lyo, R. Carr, and W. K. Ford, Phys. Rev. Lett. **58**, 207 (1987).
[11] K. Boyer, T. S. Luk, J. C. Solem, and C. K. Rhodes, Phys. Rev. A **39**, 1186 (1989).
[12] G. Gibson, T. S. Luk, A. McPherson, K. Boyer, and C. K. Rhodes, Phys. Rev. A **40**, 2378 (1989).
[13] C. Guo, M. Li, and G. N. Gibson, Phys. Rev. Lett. **82**, 2492 (1999).
[14] Q. Liang, C. Wu, Z. Wu, M. Liu, Y. Deng, and Q. Gong, Int. J. Mass Spectrom. **286**, 28 (2009).
[15] G. N. Gibson, M. Li, C. Guo, and J. P. Nibarger, Phys. Rev. A **58**, 4723 (1998).
[16] C. Cornaggia, J. Lavancier, D. Normand, J. Morellec, and H. X. Liu, Phys. Rev. A **42**, 5464 (1990).
[17] D. L. Hatten, J. Zhu, J. Goldhar, and W. T. Hill, Laser Phys. **7**, 858 (1997).
[18] H. Liu, Z. Yang, and Z. Gao, J. Chem. Phys. **126**, 044316 (2007).
[19] D. T. Strickland, Y. Beaudoin, P. Dietrich, and P. B. Corkum, Phys. Rev. Lett. **68**, 2755 (1992).
[20] V. Tagliamonti, H. Chen, and G. Gibson, Phys. Rev. A **84**, 043424 (2011).
[21] R. S. Mulliken, J. Chem. Phys. **7**, 20 (1939).
[22] S. V. Menon, J. P. Nibarger, and G. Gibson, J. Phys. B: At. Mol. Opt. Phys. **35**, 2961 (2002).
[23] I. Kawata, H. Kono, Y. Fujimura, and A. D. Bandrauk, Phys. Rev. A **62**, 031401(R) (2000).
[24] R. Polák and J. Čížek, J. Mol. Struct. **547**, 17 (2001).
[25] N. Levasseur, P. Millie, P. Archirel, and B. Levy, Chem. Phys. **153**, 387 (1991).
[26] P. Q. Wang, A. M. Sayler, K. D. Carnes, J. F. Xia, M. A. Smith, B. D. Esry, and I. Ben-Itzhak, Phys. Rev. A **74**, 043411 (2006).
[27] B. Gaire, Ph.D. thesis, Kansas State University, 2011.
[28] B. Gaire, U. Ablikim, M. Zohrabi, S. Roland, K. D. Carnes, and I. Ben-Itzhak (unpublished).
[29] H. Maschiko, C. M. Nakamura, C. Li, E. Moon, H. Wang, J. Tackett, and Z. Chang, Appl. Phys. Lett. **90**, 161114 (2007).
[30] M. Lein, J. Phys. B: At. Mol. Opt. Phys. **40**, R135 (2007).
[31] L. D. Landau, Phys. Z. Sowjetunion **2**, 46 (1932).
[32] C. Zener, Proc. R. Soc. London, Ser. A **137**, 696 (1932).
[33] A. Hishikawa, S. Liu, A. Iwasaki, and K. Yamanouchi, J. Chem. Phys. **114**, 9856 (2001).

[34] A. M. Sayler, P. Q. Wang, K. D. Carnes, B. D. Esry, and I. Ben-Itzhak, Phys. Rev. A **75**, 063420 (2007).
[35] G. Herzberg, *Spectra of Diatomic Molecules*, 2nd ed. (Van Nostrand, Princeton, 1950).
[36] T. Zuo and A. D. Bandrauk, Phys. Rev. A **52**, R2511 (1995).
[37] S. N. Dixit, D. L. Lynch, and V. McKoy, Phys. Rev. A **30**, 3332 (1984).
[38] J. H. Posthumus, B. Fabre, C. Cornaggia, N. de Ruette, and X. Urbain, Phys. Rev. Lett. **101**, 233004 (2008).
[39] C. Guo, Phys. Rev. A **73**, 041401 (2006).
[40] I. Ben-Itzhak, P. Q. Wang, A. M. Sayler, K. D. Carnes, M. Leonard, B. D. Esry, A. S. Alnaser, B. Ulrich, X. M. Tong, I. V. Litvinyuk, C. M. Maharjan, P. Ranitovic, T. Osipov, S. Ghimire, Z. Chang, and C. L. Cocke, Phys. Rev. A **78**, 063419 (2008).
[41] T. Šedivcová, P. R. Žd'ánská, V. Špirko, and J. Fišer, J. Chem. Phys. **124**, 214303 (2006).
[42] K. Okada and S. Iwata, J. Chem. Phys. **112**, 1804 (2000).
[43] P. H. Krupenie and S. Weissman, J. Chem. Phys. **43**, 1529 (1965).